applied optics

How good is your lens? Assessing performance with MTF full-field displays

Brandon Dube,[1,2,*] Roger Cicala,[1] Aaron Closz,[1] and Jannick P. Rolland[2]

[1]Olaf Optical Testing LLC, Suite 106, 7730 Trinity Road, Cordova, Tennessee 38018, USA
[2]The Institute of Optics, University of Rochester, 275 Hutchinson Road, Rochester, New York 14627, USA
*Corresponding author: brandondube@gmail.com

Received 10 April 2017; revised 11 June 2017; accepted 12 June 2017; posted 14 June 2017 (Doc. ID 292255); published 6 July 2017

Modern optical systems achieve incredible resolution and require more thorough testing. We present a method of evaluating and displaying the modulation transfer function (MTF) of a lens over its full rectangular field of view. The method consists of utilizing commercially available MTF test stations to gather data as well as custom software to plot the results. Critically, these measurements allow the characterization of misaligned systems with much higher accuracy than the typical three- or five-field-point MTF measurements yield. Examples are provided of both well-centered and poorly centered systems.

OCIS codes: (120.3940) Metrology; (120.4630) Optical inspection; (120.4800) Optical standards and testing.

https://doi.org/10.1364/AO.56.005661

1. INTRODUCTION

Optical system testing can be broken into a handful of categories. The first, camera-based target analysis testing (CTA) [1] is primarily used for quality control inspection of low-cost and/or consumer optics. It may be done either with computer measure or visual inspection of images by an operator. In both cases, it is extremely fast and suited to serial manufacture. A step above exists modulation transfer function (MTF) testing [2] and, beyond that, interferometric [3] or phase-retrieval [4] based methods of measuring the wavefront of a system and fitting it to, e.g., the Zernike polynomials [5] on a term-by-term basis. Each of these methods may be used in quality control procedures to detect bad or failed optical assemblies. Quality control testing is the focus of this paper.

Curiously, as the breadth of information gained from testing increases, generally the number of field points analyzed decreases. This is due in no small part to the greater difficulty, time, and cost associated with increasing the number of measures for these high-precision methods. While CTA may offer 50 or more measurements across the detector area, MTF measurements are typically taken at only three points (0, 7/10, and 1/1 relative field), and wavefront analysis techniques often only one.

It is important to recognize that the goal of quality control testing is to identify misaligned systems and that they will exhibit asymmetrical behaviors that can be described by nodal aberration theory (NAT) [6,7]. With this knowledge, it is a bit of a faux-pas to measure only three field points in MTF testing, or even just five if a series of measurements from left to right is made. MTF full-field displays (MTF FFDs) are inspired by the full-field display technique developed by Thompson in the 1980s to analyze optical systems without symmetry [8,9]. This technique utilizes the decomposition of a system's pupil into components (e.g., Zernike polynomials) as well as 2D plots displaying the vector behavior in the aberration fields of a system.

Figure 1 displays an MTF FFD for a lens with tilts and decenters at the extremes of its tolerances, where larger circles indicate higher MTF. If the MTF was measured along an axis from the lower left to the upper right, the lens would likely pass inspection. If it were measured along an axis from the top left to the bottom right, it would likely fail.

In the 1940s and 50s, Schade derived the optical transfer function (OTF), the modulus of which is the MTF. [10–13]. The OTF may be written as

$$\mathrm{OTF}(\nu_x, \nu_y) = |H(\nu_x, \nu_y)| \exp(i\phi(\nu_x, \nu_y)), \quad (1)$$

where $|H|$ is the MTF, ϕ is the phase transfer function (PTF), and ν_x and ν_y denote the spatial frequency associated with the x and y spatial dimensions, respectively. Note that while we do not explicitly write the normalization in our equations, the MTF is always defined to have a value of 1 and the PTF a value of 0 at the origin.

It has been shown that the OTF is the Fourier transform of the point spread function (PSF) [14],

$$\mathrm{OTF}(\nu_x, \nu_y) = \iint_{-\infty}^{\infty} \mathrm{PSF}(x, y) \exp(2\pi i \nu_x \nu_y xy) \mathrm{d}x\mathrm{d}y. \quad (2)$$

Because bright point sources are relatively uncommon, the PSF is often difficult to acquire directly. For this reason, the line

Corrected 18 July 2017

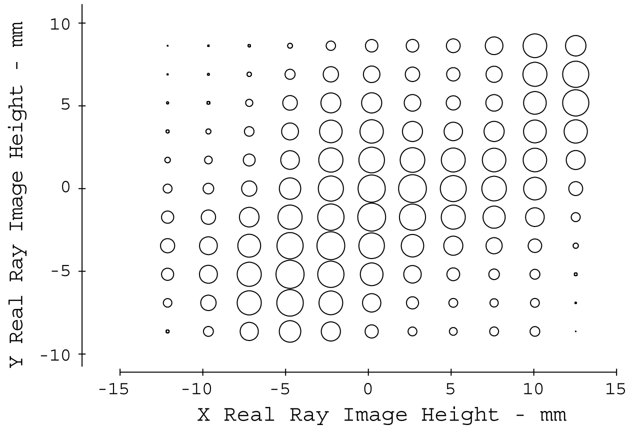

Fig. 1. MTF FFD generated using the CODE V optical design code.

spread function (LSF) [15] was derived and used to compute the PSF from a slit and also shown to yield a 1D slice of the OTF by related mathematics [16,17]:

$$\mathrm{OTF}(\nu_x) = \int_{-\infty}^{\infty} \mathrm{LSF}(x)\exp(2\pi i\nu_x x)\mathrm{d}x. \tag{3}$$

Note that LSF(x) is acquired from a slit that is oriented along the y axis. If the input is a step (e.g., a pair of black and white stripes) instead of a slit, one can measure the edge spread function (ESF), sometimes also known as the edge response function. The derivative of the ESF is the LSF:

$$\mathrm{LSF}(x) = \frac{d}{\mathrm{d}x}\mathrm{ESF}(x). \tag{4}$$

In the 1960s, it was also found that the ESF can be used to compute the MTF directly [18–20]. This property alleviates lighting concerns further still and allows a method mostly agnostic to object scale. It can be beneficial to see these relationships graphically—this is shown in Fig. 2.

These methods have evolved into a technique known as the slanted-edge method, standardized in ISO 12233 [21], which is widely used in academia, commercial software such as Imatest [22], and free open-source software such as MTF Mapper [23]. The pinhole and slit techniques are standardized in ISO 9334 and ISO 9335 [24,25] and discussed in ISO 11421 [26].

It is somewhat the norm for the slanted-edge MTF measurements to be presented on a grid or surface plot. Prior work has also been done to modify [27] or replace [28] the slanted-edge method, in which cases contour plots have also been used. It should be noted that the plots in these papers have axes in the frequency domain, while the MTF FFD has axes in the spatial domain. Additionally, Masaoka *et al.* (2014) and Arnison *et al.* (2011) focused their investigation along or near the optical axis of the lens [27,28].

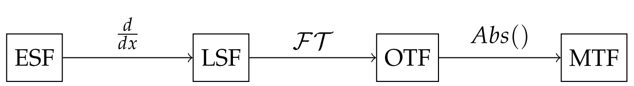

Fig. 2. Block diagram of the mathematical relationships between various representations of an image. $\mathcal{FT}$ represents the Fourier transform.

Full-field measurement techniques have not yet been applied to MTF measurements made via the slit or pinhole methods, which are utilized by the MTF benches offered by commercial vendors. Optical systems are higher resolution than ever with tight tolerances. If a system is tested to meet specifications at three field points, it may fail elsewhere in the field of view (FOV). The FFD technique is able to find these systems, where typical measurements using three or five field points in a line may miss them.

The ultra-high resolution of today's optical systems requires robust metrology. In the consumer space, end users have become sensitive to asymmetric image quality in digital single lens reflex (DSLR) and mirrorless camera lenses, as well as cell phone cameras. This is a symptom of optical misalignment, which for many manufacturers goes undetected at the factory as a consequence of lesser quality metrology.

In the professional video and cinema market 4K, 6K, and 8K Super35, Full-Frame, or VistaVision cameras with 4 μm or smaller pixels are becoming increasingly common. These high-resolution sensors no longer mask the defects of objective lenses the way 1080p or lower-resolution cameras have in the past.

The majority of the industrial optics landscape has not increased in resolution as rapidly as the consumer market, outside of specialty areas like satellite imagers. Instead, specifications have become more extreme in areas like size, driven by the use of aspheric and freeform optics [29]. Component-level metrology has increased in capabilities with tools, such as stitching interferometers, being developed to handle the testing of these surfaces [30,31]. System level metrology has been left behind.

It should be noted that there is emerging technology addressing the need for advanced system-level metrology. Commercial test platform vendors such as Optikos and Trioptics have recently released multi-field test stations [32,33]. These systems are able to identify severe misalignment, and while the number of field points tested is generally less than 10 and may not address the need to quantify small misalignments, these advances offer the benefit of testing at multiple field points simultaneously.

2. GATHERING DATA AND PLOTTING

The software accompanying most MTF test stations computes the MTF by the pinhole or slit method and defaults to plotting a 1D MTF as a function of spatial frequency with dashed and solid traces plotted for the tangential and sagittal planes of each field point. With just three points, these are legible, but when many field points are measured, they become all but unreadable. An example of this type of plot is given in Fig. 3 for 21 points equally spaced along each of four slices in the FOV. Raw numerical data are even more difficult to parse. Many commercial lens manufacturers publish plots of the MTF at select spatial frequencies against image height for their lenses. Some MTF test stations feature this type of plot out of the box. Rotational symmetry is implied by these plots, but any misaligned optical assembly has lost that property to some degree.

One method to quantify the MTF across the full FOV is to measure several slices through the full FOV at different azimuthal

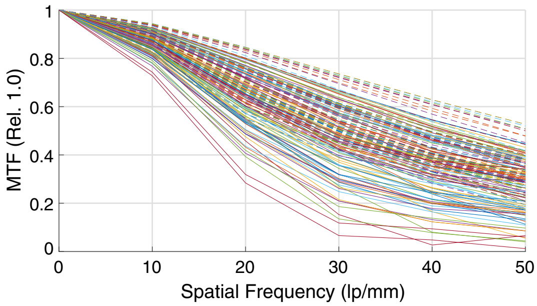

Fig. 3. Plot of the MTF as a function of spatial frequency for the 81 field points measured. Solid lines tangential, dashed lines sagittal MTF. A legend is omitted, as 81 entries would be unreasonable.

angles and plot each scan independently. This is also the technique we use to gather the data for a FFD. Figure 4 shows the layout of these slices in the area of a detector, and Fig. 5 displays an example of this type of plot for a measure taken across four slices. The largest issue with this type of display is that the field dependency of the MTF is difficult to discern. MTF FFDs solve this issue. Additionally, if many slices are measured, it takes significant time to digest the plots. MTF FFDs provide a visualization that can be understood quickly.

By bookkeeping the angle θ, the numerical data can be expressed as a 3D function of (h, θ, ν) where h is the image height, θ is the azimuth in the image plane as noted in Fig. 4, and ν is the spatial frequency. The horizontal and vertical components can be extracted with a transformation from polar to Cartesian coordinates.

Because the data is 3D and a surface or contour plot is 2D, one variable must be fixed. As we are interested in field-dependent behavior, we strategically fix the spatial frequency. Then, four different MTF FFDs may be plotted where each 2D plot corresponds to the MTF in the tangential or sagittal direction or combines data from multiple axes of the MTF. One may plot the tangential or sagittal MTFs over the full FOV, both of which are intuitive and will invite direct comparison to MTFs computed by an optical design code (e.g., CODE V, Zemax, or OSLO). One may also plot the average (T&S) of the tangential and sagittal MTFs, which is often useful to reduce the information to one image. There is also the difference (T&S), defined as the difference between the tangential and sagittal MTFs.

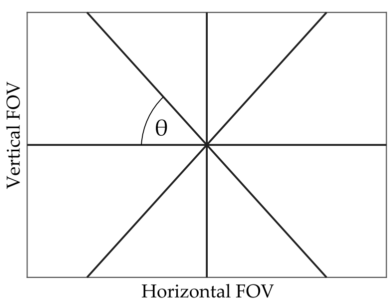

Fig. 4. Each line represents a slice along which the MTF is measured at several points. The angle θ is the clocking angle between rotations. In this example, $\theta = 45°$.

If the lens will take pictures for human consumption, low spatial frequencies should be analyzed in addition to high spatial frequencies. A significant amount of the subjective quality of an image is determined by the contrast at low to mid spatial frequencies, as discussed by Granger and Cupery (1972) and Hultgren (1990) [34,35].

One may use a wide range of software to generate a surface plot to represent the data. In some packages, the surface may be interpolated between measured points by a range of different methods. Linear interpolation is used in the plots shown. The resulting surface should be encoded in color, and consideration must then be given to the choice of the colormap. In most examples, jet has been purposefully used because it significantly changes tone in nearly 10% increments of the plotted value, which is in-sync with what is a significant change in the value of the MTF. While perhaps not well known by name in the optics community, jet is a colormap that has been the default in MATLAB and plotting tools for over 20 years and fits these criteria. The difference (T&S) MTF FFDs utilize a diverging red-blue colormap centered at 0 due to the significance of both the magnitude and sign of the departure from zero.

Time, versatility, and cost are important factors that play into the metrology decisions for an optical system. While MTF FFDs cannot be generated in the seconds it takes to do serial testing of a lens model with CTA or the slanted-edge method (after initial alignment of the camera to the test chart), they provide higher-quality measurements and do not tie the test to any one detector and its associated Nyquist limit. Even with the oversampling implemented by the slanted-edge method to help extend the Nyquist limit of the camera, ultimately the effective Nyquist limit of the camera fundamentally imposes some limitation. For lenses that feature a common mechanical interface, for example C mount, higher resolution cameras will likely be used in the future. Full-field displays are also derived from data that can be gathered *much* faster than interferometric or phase-retrievalbased techniques. They also do not require specific aids (such as pellicle attenuators used in interferometry) other than a motorized mount capable of rotation holding the lens under test, which is an accessory already commonly featured on commercial MTF benches.

With 21 measurements each in four slices, measurement times utilizing a commercial test station range from approximately 15 min for a wide-angle model to 4 min for a telephoto model. This may be compared to the hours, if not days, necessary to make several off-axis interferometric measurements.

3. RESULTS

Figure 5 shows the MTF as a function of field for four slices and the same lens as Fig. 3. Commercial lens manufacturers typically provide these plots with the x axis ranging from 0 to the maximum image height for the image format. Our plot shows the full symmetric scan through the FOV that is made. These manufacturer-provided charts have implicit rotational symmetry, but this is rarely the case for an assembled lens.

Figure 6 shows the MTF FFDs for the same lens as Fig. 5; they are highly asymmetric, and the field dependence of the MTF is easy to grasp. We wish to emphasize that this lens *should* be rotationally symmetric, but after it is assembled,

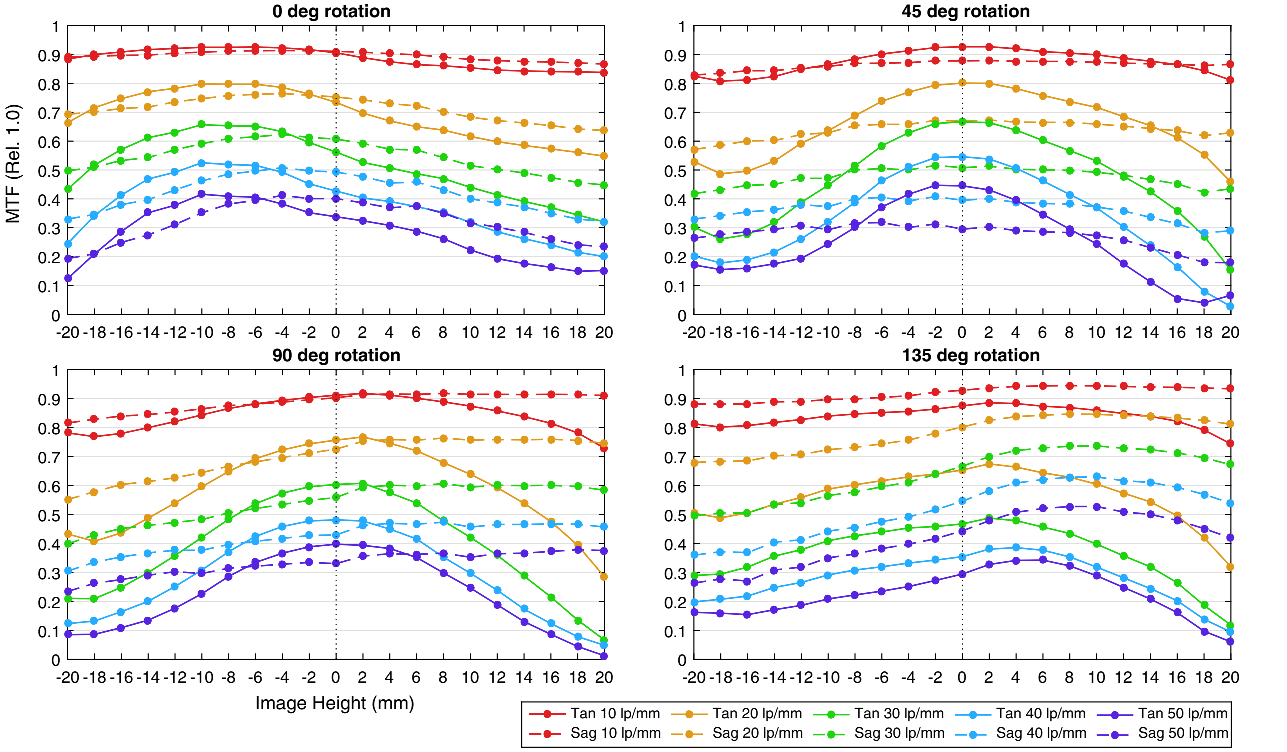

Fig. 5. Example of a plot of MTF versus field for each of four azimuths. This type of display is information dense and is neither intuitive nor quick to read.

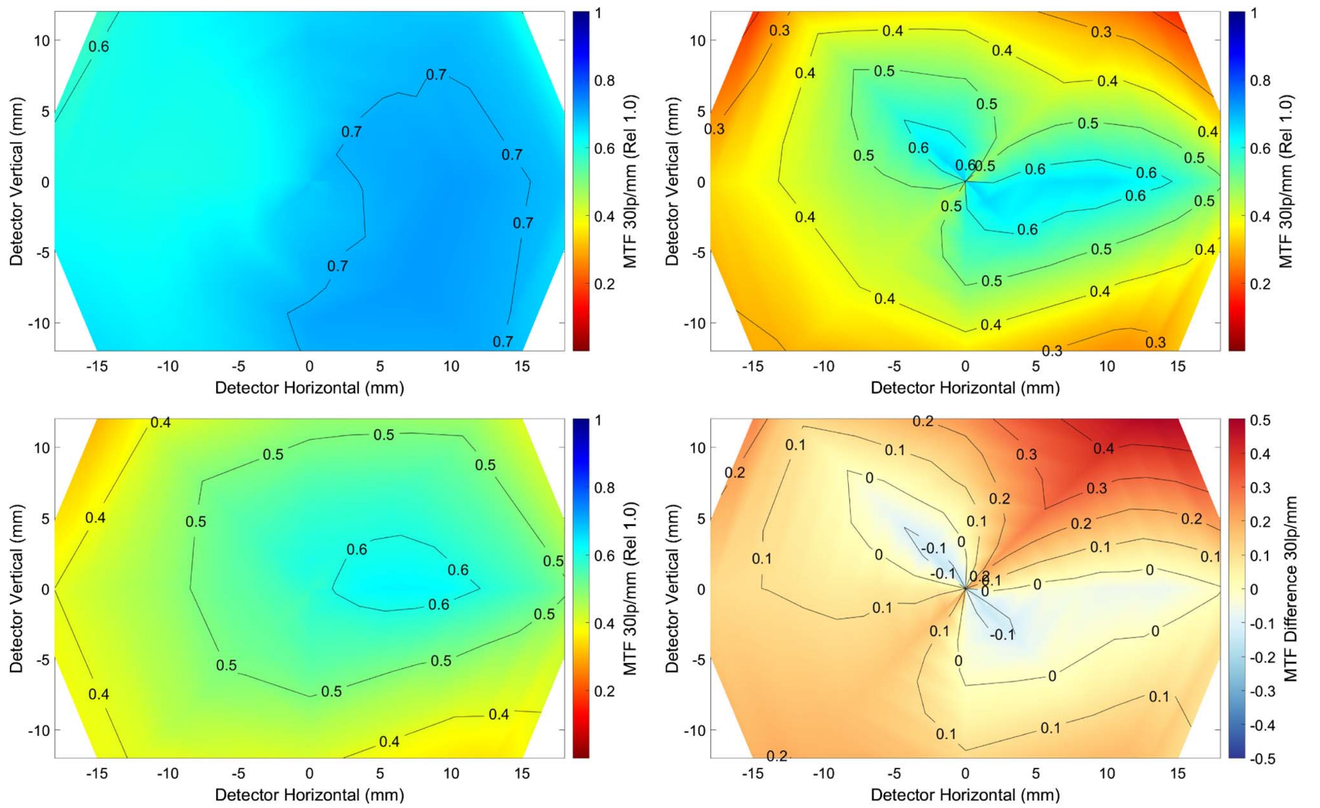

Fig. 6. Example of the four types of MTF FFDs, from left to right, top to bottom: sagittal, tangential, average (T&S), difference (T&S). This lens is not well aligned, but this type of behavior is (surprisingly) extremely common.

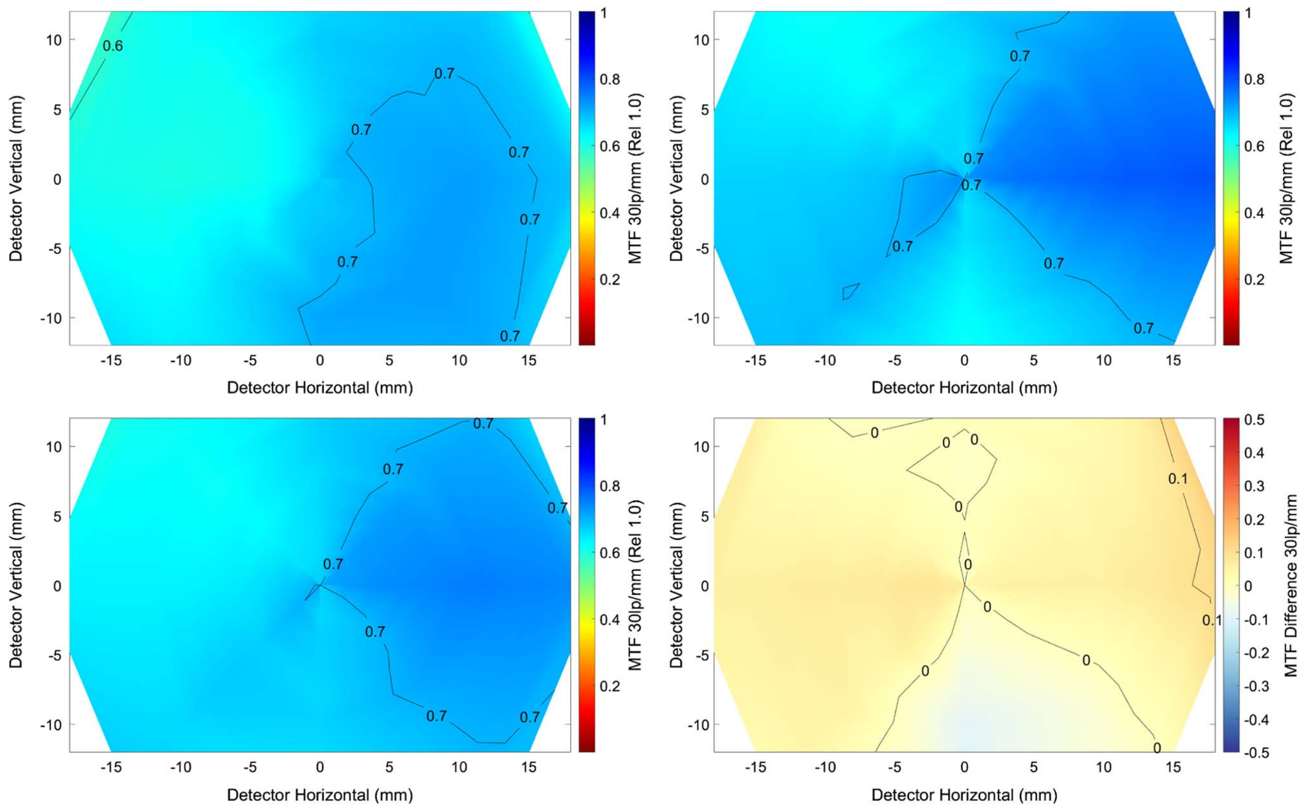

Fig. 7. Example of the four types of MTF FFDs, from left to right, top to bottom: sagittal, tangential, average (T&S), difference (T&S). This lens is well aligned.

the alignment errors create substantial asymmetry in its performance. Figure 7 is the same as Fig. 6, but for a well-centered lens of the same model as tested in Fig. 6. It has been the assumption for decades of slit- or pinhole-based MTF testing that all tested lenses behave this way. In applying our method to over 2000 individual commercial lenses with prices ranging

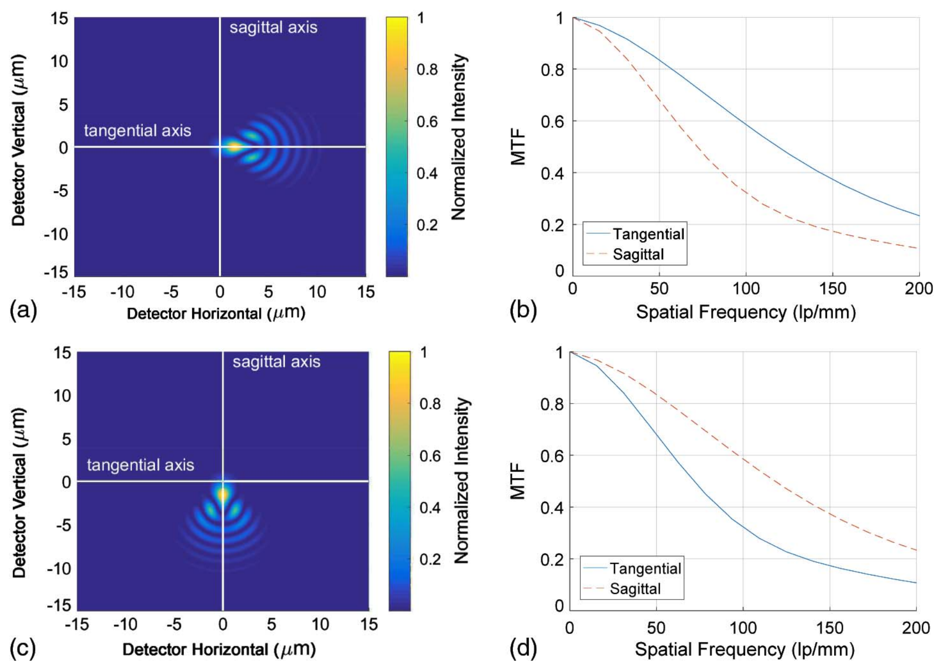

Fig. 8. (a) and (b) Nominal rotation of the lens under test, (c) and (d) after 90° rotation. The rotation is performed to measure the MTF for various azimuths of the lens under test. This spot or PSF was taken to lie on the optical axis of the lens, and the coma results from misalignment.

from \$125 to \$42,750, we have found that less than 10% of lenses have this quality.

Figure 8 shows the PSF and MTF for a nominally symmetric 50 mm f/2 lens with 1 wave 0-to-peak of Seidel coma observed for a point on axis and generated by misalignment at two azimuths of the lens under test. Note that in our instrument, the slit can be placed at any location within the full FOV of the lens by a combination of a rotation of the object generator assembly and an azimuthal rotation of the lens under test. With this convention, the tangential and sagittal axes associated with a point in the field are always referenced to the x and y axes of the image plane. As a consequence, any asymmetric aberration, coma being the most prominent, will yield tangential and sagittal MTFs that depend on the azimuth of the lens, as exemplified in Fig. 8.

4. HOW MANY SLICES ARE ENOUGH?

The number of slices in the FOV has some importance. The aforementioned three- and five-field-point measurements constitute one half and one full slice, respectively. It is impossible to generate an MTF FFD from only a single slice, and two slices would result in extreme interpolation. Three slices prevent one from making measurements along the cardinal axes. It is for these reasons we choose four slices for a standard. More are always possible; however, we do not find more to be useful in the majority of cases. Here, we show a progression from four slices to 12 for a misaligned lens. If the lens behaved in a way that was rotationally symmetric (i.e., was well aligned) it would not make a good case study, as we do not expect a difference at different azimuths in the field under the assumption of rotational symmetry. It can be seen in the figures that even in a system without rotationally symmetric behavior, four slices faithfully reveal the field dependent behavior of the MTF. Critically, there are no new extrema revealed by increasing the data density. If there appeared to be an area of high gradient in the MTF, more slices may be justified, as there is risk of missing the extrema in the scan.

In this example, the three plots in Fig. 9 are similar, and the essence of the performance is faithfully obtained by measuring four slices. Eight- and 12-slice MTF FFDs show only smaller ripples. An increase from 12 to (for example) 25 slices does not yield significantly more information. All of the plots are made from data collected in separate measurements and did not utilize any smoothing techniques except for linear interpolation between measured points. The difference (T&S) FFD was chosen, as it compounds the tangential and sagittal MTFs in a way that is very sensitive to any gradient in the tangential and sagittal MTFs as a function of field, as well as departures from rotational symmetry.

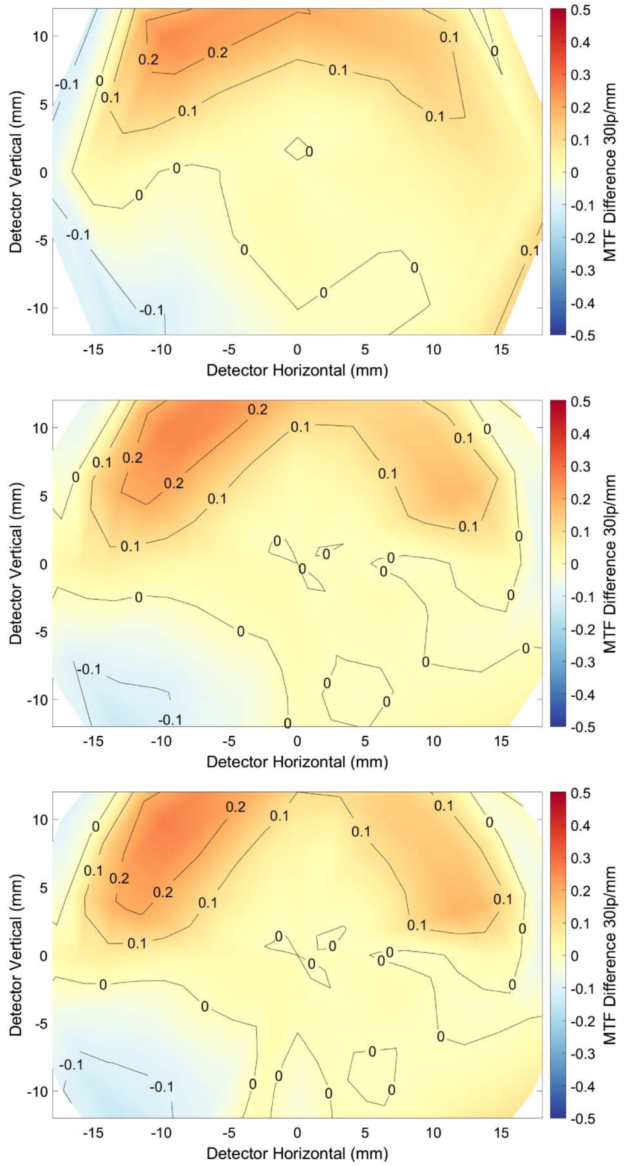

Fig. 9. Set of difference (T&S) MTF FFDs generated based on measurements across four, eight, and 12 azimuths of the lens under test's full FOV.

5. DISCUSSION

The MTF FFDs cannot provide the same depth of information regarding the quantification of specific aberrations as phase-retrieval or interferometric methods. However, it is possible to estimate which drive performance based on the nominal residual aberrations of the lens under test combined with software simulations. One may also go back after generating each of the MTF FFDs and capture the PSF or LSF from the lens under test, or measure the wavefront at points of interest. This allows diagnosis of the alignment errors of the system without spending excess time measuring the PSF or wavefront systematically across the full field.

As the image height increases, the distance between data points of different slices increases. Stated differently, the measurement density near the optical axis is much higher than the edge of the field. The software that operates the MTF bench could easily be modified to include an algorithm for uniform sampling across a rectangular FOV.

In a sufficiently disturbed system, the on- and very-near-axis measurements will fluctuate, based on the relative quantity of vertical and horizontal coma (corresponding to fringe Zernike terms Z7 and Z8) present and/or the clocking angle of the astigmatism, as in Fig. 8.

When synthetic surfaces are displayed, discontinuities or jagged plots may result, which are visually displeasing. The average (T&S) of all slices at an image height of 0 may be used to alleviate the issue and is usually sufficient. Mild smoothing algorithms may be run on the near-axis region to remove sharp local discontinuities. It is uncommon for this region to present the largest issues, so this is also typically acceptable, but it is not advised for displaying systems with tight tolerances.

6. CONCLUSION

We have presented a method of utilizing commercial instruments to measure the MTF of a lens over the full FOV. This method allows a more complete evaluation of as-built performance, and misalignment is readily visualized.

While assumptions about rotational symmetry are valid in the controlled context of optical design, they often do not hold when an optical system is assembled, or after handling and transport. Rotationally symmetric systems are best tested across their full FOV to ensure their performance is rotationally symmetric. The MTF FFDs are an effective means to this end that leverages existing technology.

Funding. Robert E. Hopkins Center at the Institute of Optics, University of Rochester (UR).

Acknowledgment. Additional support in performing testing and developing these techniques was provided by Olaf Optical Testing. The tested lenses were provided by Lensrentals.com as part of its new item inspection pipeline. Additionally, we would like to thank Synopsys for the student license of CODE V utilized in generating Fig. 1. We would also like to thank Optikos for stimulating discussion and production of a custom instrument that has proven invaluable to this research. Lastly, we would like to thank Trioptics for the production of our ImageMaster HR bench, on which we have taken the measurements to produce the MTF FFDs seen in this paper.

REFERENCES

1. "Mil-std-150a photographic lenses," (1959).
2. P. T. Carellas and S. D. Fantone, "Why measure MTF?" Opt. Photon. News **1**(6), 27–29 (1990).
3. D. Malacara, *Optical Shop Testing*, 3rd ed. (Wiley, 2007).
4. J. R. Fienup, "Phase retrieval algorithms: a comparison," Appl. Opt. **21**, 2758–2769 (1982).
5. F. Zernike, "Beugungstheorie des schneidenver-fahrens und seiner verbesserten form, der phasenkontrastmethode," Physica **1**, 689–704 (1934).
6. K. P. Thompson, "Aberration fields in tilted and decentered optical systems," Ph.D. thesis (University of Arizona, 1980).
7. K. Thompson, "Description of the third-order optical aberrations of near-circular pupil optical systems without symmetry," J. Opt. Soc. Am. A **22**, 1389–1401 (2005).
8. K. P. Thompson, "A graphic approach to the analysis of perturbed optical systems," Proc. SPIE **0237**, 127–134 (1980).
9. K. P. Thompson, "Beyond optical design interaction between the lens designer and the real world," Proc. SPIE **0554**, 426–438 (1986).
10. O. Schade, "Electro-optical characteristics of television systems. Introduction and part I: characteristics of vision and visual systems," RCA Rev. **9**, 5–37 (1948).
11. O. Schade, "Electro-optical characteristics of television systems, part II: electro-optical specifications for television systems," RCA Rev. **9**, 245–286 (1948).
12. O. Schade, "Electro-optical characteristics of television systems, part III: electro-optical characteristics of camera systems," RCA Rev. **9**, 491 (1948).
13. O. Schade, "Electro-optical characteristics of television systems, part IV: correlation and evaluation of electro-optical characteristics of imaging systems," RCA Rev. **9**, 653–686 (1948).
14. H. H. Hopkins, "The frequency response of optical systems," Proc. Phys. Soc. London Sect. B **69**, 562–576 (1956).
15. R. Barakat and A. Houston, "Line spread function and cumulative line spread function for systems with rotational symmetry," J. Opt. Soc. Am. **54**, 768–773 (1964).
16. E. W. Marchand, "Derivation of the point spread function from the line spread function," J. Opt. Soc. Am. **54**, 915–919 (1964).
17. E. W. Marchand, "From line to point spread function: the general case," J. Opt. Soc. Am. **55**, 352–354 (1965).
18. F. Scott, R. M. Scott, and R. V. Shack, "The use of edge gradients in determining modulation transfer functions," Photogr. Sci. Eng. **7**, 64–68 (1963).
19. B. Tatian, "Method for obtaining the transfer function from the edge response function," J. Opt. Soc. Am. **55**, 1014–1019 (1965).
20. R. Barakat, "Determination of the optical transfer function directly from the edge spread function," J. Opt. Soc. Am. **55**, 1217–1221 (1965).
21. "Photography–Electronic still picture imaging–Resolution and spatial frequency responses," ISO standard 12233:2017 (2017).
22. Imatest, 2017, http://imatest.com.
23. Mtf Mapper, 2017, https://sourceforge.net/projects/mtfmapper/.
24. "Optics and photonics–Optical transfer function–Definitions and mathematical relationships," ISO standard 9334:2012.
25. "Optics and photonics–Optical transfer function–Principles and procedures of measurement," ISO standard 9335:2012.
26. "Optics and optical instruments–accuracy of optical transfer function (OTF) measurement," ISO standard 11421:1997.
27. K. Masaoka, T. Yamashita, Y. Nishida, and M. Sugawara, "Modified slanted-edge method and multidirectional modulation transfer function estimation," Opt. Express **22**, 6040–6046 (2014).
28. M. R. Arnison, D. P. Morgan-Mar, C. A. Deller, P. A. Fletcher, and K. G. Larkin, "Measurement of the lens optical transfer function using a tartan pattern," Appl. Opt. **50**, 2158–2169 (2011).
29. K. P. Thompson and J. P. Rolland, "Freeform optical surfaces: a revolution in imaging optical design," Opt. Photon. News **23**(6), 30–35 (2012).
30. Y.-M. Liu, G. N. Lawrence, and C. L. Koliopoulos, "Subaperture testing of aspheres with annular zones," Appl. Opt. **27**, 4504–4513 (1988).
31. P. E. Murphy, G. W. Forbes, J. F. Fleig, D. Miladinovic, G. DeVries, and S. O'Donohue, "Recent advances in subaperture stitching interferometry," in *Frontiers in Optics* (Optical Society of America, 2006), paper OFWC2.
32. "Meridian production camera test system," 2017, http://optikos.com.
33. "Imagemaster pro 9," 2017, http://trioptics.com.
34. E. Granger and K. Cupery, "An optical merit function (SQF), which correlates with subjective image judgements," Photogr. Sci. Eng. **15**, 221–230 (1972).
35. B. O. Hultgren, "Subjective quality factor revisited: a unification of objective sharpness measures," Proc. SPIE **1249**, 12–22 (1990).